Active regulation of the epidermal calcium profile

M.P. Adams[a,*], D.G. Mallet[a], G.J. Pettet[a]

[a] *Discipline of Mathematical Sciences, Faculty of Science and Technology, and Institute of Health and Biomedical Innovation, Queensland University of Technology, GPO Box 2434, Brisbane 4001, Australia*

Abstract

A distinct calcium profile is strongly implicated in regulating the multi-layered structure of the epidermis. However, the mechanisms that govern the regulation of this calcium profile are currently unclear. It clearly depends on the relatively impermeable barrier of the stratum corneum (passive regulation) but may also depend on calcium exchanges between keratinocytes and extracellular fluid (active regulation). Using a mathematical model that treats the viable sublayers of unwounded human and murine epidermis as porous media and assumes that their calcium profiles are passively regulated, we demonstrate that these profiles are also actively regulated. To obtain this result, we found that diffusion governs extracellular calcium motion in the viable epidermis and hence intracellular calcium is the main source of the epidermal calcium profile. Then, by comparison with experimental calcium profiles and combination with a hypothesised cell velocity distribution in the viable epidermis, we found that the net influx of calcium ions into keratinocytes from extracellular fluid may be constant and positive throughout the stratum basale and stratum spinosum, and that there is a net outflux of these ions in the stratum granulosum. Hence the calcium exchange between keratinocytes and extracellular fluid differs distinctly between the stratum granulosum and the underlying sublayers, and these differences actively regulate the epidermal calcium profile. Our results also indicate that plasma membrane dysfunction may be an early event during keratinocyte disintegration in the stratum granulosum.

Keywords: Epidermis, epithelium, porous medium, calcium profile, calcium gradient

1. Introduction

The epidermis is the most superficial skin layer and it possesses a distinct calcium distribution [1] which is strongly implicated in regulating its structure

*Corresponding author

Email addresses: mp.adams@qut.edu.au (M.P. Adams), dg.mallet@qut.edu.au (D.G. Mallet), g.pettet@qut.edu.au (G.J. Pettet)

[2]. Here, we investigate the epidermal calcium profile with a mathematical model and demonstrate that this profile is actively regulated.

1.1. The epidermis and its structure

Keratinocytes, which are the primary cells of the epidermis [3], differ in shape and function with depth from the skin surface. These differences characterise four sublayers of the epidermis. From deep to superficial, these sublayers are [4]:

1. *The stratum basale (SB):* Keratinocytes proliferate and possess near-cuboidal shape.
2. *The stratum spinosum (SS):* Non-proliferating keratinocytes passively migrate towards the skin surface, displaced from the SB by proliferation there.
3. *The stratum granulosum (SG):* Keratinocytes become flattened and disintegrate, expelling their contents into the extracellular space.
4. *The stratum corneum (SC):* Denucleated keratinocytes, called corneocytes, are highly flattened and surrounded by lipids that were expelled during the disintegration in the SG. The SC is responsible for the skin's barrier function [5]. Towards the skin surface, the corneocyte/lipid structure has reduced adhesion and is sloughed during everyday activity [6].

The thickness of the epidermis is homeostatically maintained at a constant, which decreases slowly over the human lifetime [7], as a result of the balance of proliferation in the SB with sloughing in the SC. Thus, the epidermis is dichotomous in that *dynamic* mechanisms - cell proliferation, passive migration, and removal - yield relatively *static* histology.

1.2. Calcium in the epidermis

The transition of keratinocytes between the epidermal sublayers, with the attended phenotypic changes called differentiation, is regulated by several signals, but a "key epidermal regulator" so far eludes determination [3]. Calcium, the Notch signalling pathway and transforming growth factor-β have been investigated for this role [8]. Calcium has been described as a "grand-master cell signaler" [9] because of its importance in multiple biological systems, and this role of calcium is an active research area of theoretical biology today [10, 11].

In unwounded epidermis, the calcium distribution possesses a profile as illustrated by Figure 1: low levels in the SB, rising gradually towards a peak in the SG, and dropping sharply to negligible levels in the SC [1]. Calcium levels are also slightly higher in the underlying dermis than in the SB [12]. The calcium profile is implicated in regulating the structure of the epidermis as basal *in vitro* keratinocytes respond to calcium by forming multi-layered structures similar to those seen *in vivo* [2].

The epidermal calcium profile is a summation of calcium from three different localisations: the extracellular fluid (ECF), the cytosol, and intracellular organelles [13] such as the endoplasmic reticulum [14] and Golgi apparatus [15].

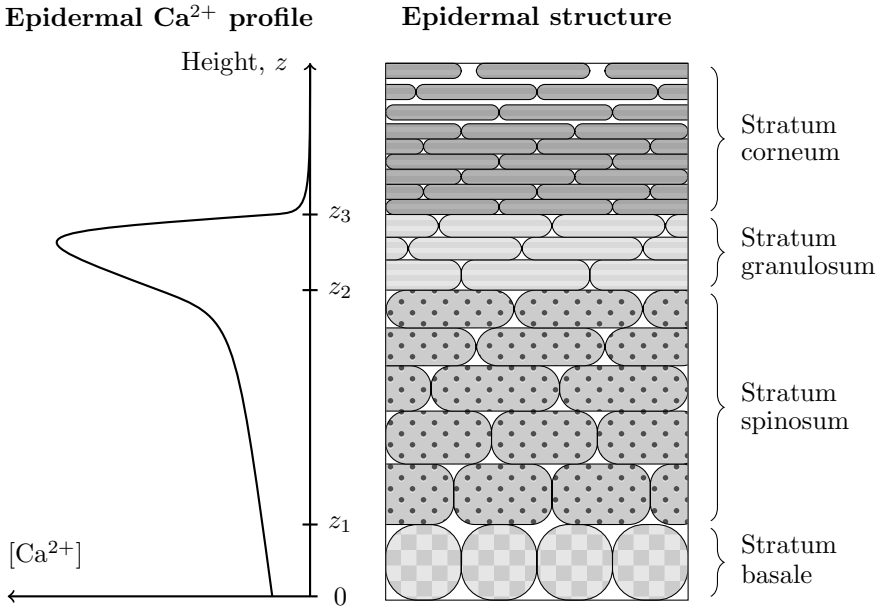

Figure 1: Schematic of the calcium profile (left) and multi-layered structure (right) of the epidermis.

To date, the specific contributions of these three localisations to the calcium profile have only been reported semi-quantitatively [16]. However, it is known that ECF [17] and organelle calcium concentrations [18] are significantly higher than in the cytosol. These concentration differences are maintained by calcium pumps, present on membranes of the keratinocytes and their intracellular structures, which actively remove calcium from the cytosol [19].

Currently, there is debate in the literature over whether the formation of the calcium profile is actively regulated [20]. It is already clear that the profile is *passively* regulated by the relatively impermeable SC, since wounding this sublayer obliterates the calcium profile [21]. However, if the profile is also *actively* regulated, changes in the action of the calcium pumps on keratinocytes membranes may contribute to formation of this profile. Celli *et al.* [22] have suggested that an active mechanism is required to keep calcium levels in the SB and SS lower than in the underlying dermis and overlying SG.

1.3. Mathematical modelling of the epidermal calcium profile

The epidermal calcium profile has been previously modelled by Cornelissen *et al.* [23]. They found that the shape of the calcium profile is mostly determined by bound calcium, and that the free calcium distribution in the viable sublayers is regulated by electrophoresis. This bound calcium may be attached to calcium-binding molecules and intracellular organelles, the latter of which

move towards the skin surface within the keratinocytes they are present. However, this bound calcium is assumed to be stationary [23], which contradicts the constant keratinocyte motion. Also, a cubic function for calcium binding sites is used, but this function is based on calcium profile data [24] rather than binding site data. An agent-based simulation by Grabe and Neuber [25] also simulates the epidermal calcium distribution, but their model assumes preferential upwards motion of calcium from cell to cell to achieve this result.

In this paper, we present a model of the viable layers of the epidermis as a saturated porous medium with keratinocytes and ECF considered analogous to soil particles and water. We use this model to predict the calcium exchange between keratinocytes and ECF as a function of skin depth in unwounded epidermis, based on experimental calcium profile data, and discuss the implications of our results. Our work suggests that diffusion may govern the extracellular calcium distribution and hence intracellular calcium is the main source of the epidermal calcium profile. This in turn indicates that differences in calcium exchange between keratinocytes and ECF with skin depth actively regulate the epidermal calcium profile. We then quantify these differences, finding possibly constant calcium influx into keratinocytes in the stratum basale and stratum spinosum, and calcium outflux from keratinocytes in the stratum granulosum. Our results also suggest that membrane dysfunction may be an early event during keratinocyte disintegration in the stratum granulosum.

2. Background

2.1. Model equations

We model the viable epidermal sublayers of the epidermis as a saturated porous medium. A variety of biological applications have been modelled as porous media, including tumour growth [26], blood flow in human tissues [27], drug delivery to the brain [28], food processing [29] and tree water flow [30].

In our model, cells and ECF co-exist at every spatial point. This continuum approach is more computationally efficient than cell population models, but loses predictive power at the individual cell level. Fozard *et al.* [31] recently evaluated the correlation between continuum and cell population models for epithelial monolayers, and suggested that continuum models are predictive for monolayers containing as few as five cells. Viable murine and human epidermis possess 4-6 [32, 33] and 5-12 [4] cell layers respectively, each layer itself consisting of vast numbers of cells. Hence we believe that modelling the viable epidermis as a porous medium is quite appropriate.

The model consists of keratinocytes, ECF and calcium, in the viable epidermal sublayers. We consider only one spatial direction z perpendicular to the skin surface. The epidermal sublayers are defined as follows: the SB in $0 \leq z \leq z_1$, the SS in $z_1 < z \leq z_2$ and the SG in $z_2 < z \leq z_3$ (see Figure 1).

As a porous medium, we consider keratinocytes analogous to soil particles and the surrounding ECF analogous to the water that saturates the soil system. Keratinocytes are treated as bags of incompressible, inviscid fluid. The ECF

surrounding the keratinocytes is assumed to possess identical properties to this cellular fluid. Calcium is always dissolved in the cells or ECF. Calcium contained in the cytosol and intracellular organelles of cells are considered together simply as intracellular calcium. Experimentally, intracellular calcium waves are known to propagate between adjacent keratinocytes [34], but these waves have insignificant magnitude compared to the calcium profiles we investigate. Hence we confine intracellular calcium to individual keratinocytes, with its velocity equal to the local keratinocyte velocity.

Unwounded epidermis varies slowly in thickness during the human lifetime [7]. The epidermal sublayers and calcium profile should be similarly stable. Hence, the epidermis is at steady state, and time dependence can be removed. With all of the above considerations in mind, the equations of our model are derived from mass conservation equations for the fluid and calcium, and are given by

$$\frac{\mathrm{d}}{\mathrm{d}z}\left(\phi u_i(z)\right) = f(z), \tag{1a}$$

$$\frac{\mathrm{d}}{\mathrm{d}z}\left((1-\phi) u_e(z)\right) = -f(z), \tag{1b}$$

$$\frac{\mathrm{d}}{\mathrm{d}z}\left(\rho_{ci}(z) u_i(z)\right) = g(z), \tag{1c}$$

$$\frac{\mathrm{d}}{\mathrm{d}z}\left(\rho_{ce}(z) u_{ce}(z)\right) = -g(z), \tag{1d}$$

where ϕ is the cell volume fraction, $1-\phi$ is the ECF volume fraction, ρ_{ci} and ρ_{ce} are the superficial intracellular and extracellular calcium concentrations respectively, u_i, u_e and u_{ce} are the physical velocities of the cells, ECF and extracellular calcium respectively, f is the rate of change of cell volume fraction due to transformation of ECF to cells, and g is the rate of change of superficial intracellular calcium concentration due to calcium transfer from ECF to cells. A schematic of the model is presented in Figure 2, in two spatial dimensions rather than one for clarity.

In its current state, system (1) is underdetermined. In saturated porous medium models of avascular tumours [26], this is rectified by including pressure or force-balance equations [35] derived from a modified version of Darcy's law [36]. However, the cell volume fraction ϕ is constant in the viable epidermal sublayers [37], and we will later specify ϕ, f, u_{ce} and $\rho_{ce} + \rho_{ci}$. This closes the model as we are left with four unknowns (u_i, u_e, g and one of ρ_{ce}, ρ_{ci}) in four equations. Hence we avoid the need of additional equations. The key result of these solutions is the calculation of g, which we use to identify any sublayer-specific differences in the calcium transfer between cells and ECF in the viable epidermis.

2.2. Boundary conditions

Keratinocytes cannot enter or exit the epidermis through the basement membrane (BM) that separates the epidermis and dermis. Hence the cell velocity

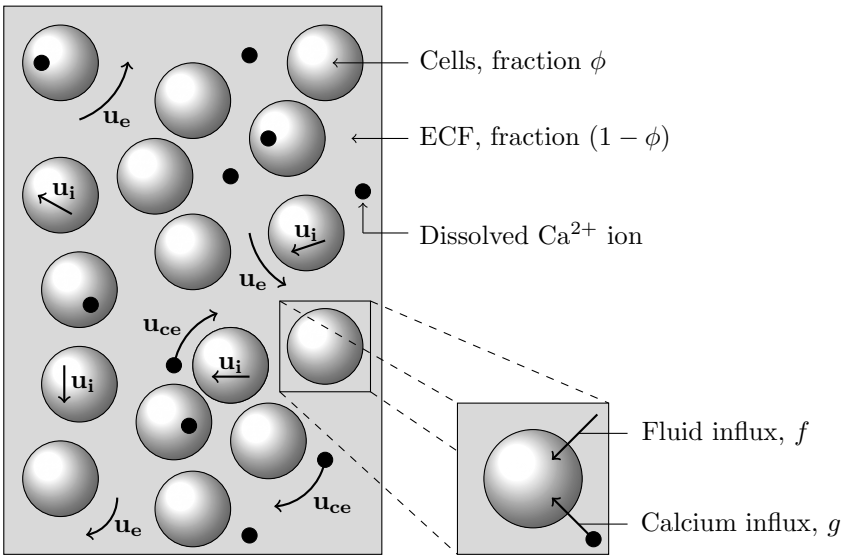

Figure 2: A schematic of the saturated porous medium model in two spatial dimensions, illustrating the flows of cells ($\mathbf{u_i}$), ECF ($\mathbf{u_e}$) and extracellular calcium ions ($\mathbf{u_{ce}}$).

through the BM is zero,

$$u_i(0) = 0, \tag{2}$$

Similarly, intracellular calcium cannot travel across the BM because it is contained within keratinocytes,

$$\frac{\mathrm{d}\rho_{ci}}{\mathrm{d}z}(0) = 0. \tag{3}$$

The calcium present in the epidermis originates from movement of fluids and calcium across the BM [38]. Hence at steady state, the BM acts as a constant source of calcium,

$$\rho_{ce}(0) = \rho_0, \tag{4}$$

where ρ_0 is the constant superficial extracellular calcium concentration at the BM. This boundary condition is appropriate if the epidermal and dermal histologies are static (e.g. unwounded skin). However, it may require reconsideration if the epidermal structure is changing (e.g. during wound healing), as calcium motion across the BM increases in response to wounding of the epidermis [21].

The SC is relatively impermeable to water transport [39]. Hence the flow of ECF through the SG-SC interface is negligible,

$$u_e(z_3) = 0, \tag{5}$$

and extracellular calcium cannot travel across this interface because it is dissolved in the ECF,

$$\frac{\mathrm{d}\rho_{ce}}{\mathrm{d}z}(z_3) = 0. \tag{6}$$

This boundary condition represents the assumption of passive regulation of the calcium profile.

At the sublayer boundaries z_1 and z_2, all volume fractions and velocities are continuous. The ρ_{ce} profile and its gradient are also continuous at these boundaries because the ECF is contiguous. However, ρ_{ci} and its gradient are not generally continuous because its distribution spans multiple cells, so spatially adjacent points in the domain may possess independent ρ_{ci} values.

3. Results

3.1. Cell and fluid velocities in the viable epidermis

Next, we specify $f(z)$ in the different sublayers, based on information from the experimental literature.

1. *The stratum basale,* $0 \leq z \leq z_1$: Keratinocytes proliferate at a rate that is assumed constant per cell volume, based on the observation that *in vitro* keratinocytes proliferate at an exponential rate until a confluent monolayer forms [40]. Although there is evidence [41] for separate stem and transit-amplifying cell subpopulations possessing different proliferation rates in the SB, the slow-cycling stem cells compose only 1-10% of this sublayer [42] and so may not significantly affect the proliferation kinetics.
2. *The stratum spinosum,* $z_1 \leq z \leq z_2$: Keratinocytes do not proliferate or disintegrate, and keratinocyte volume change is small [43]. Hence we assume that there is no significant cellular fluid influx in this sublayer.
3. *The stratum granulosum,* $z_2 \leq z \leq z_3$: Keratinocytes disintegrate and reduce in size. We assume that this disintegration occurs at a constant rate per cell volume for simplicity.

As a simple representation of the assumptions given above, we define the following form of $f(z)$,

$$f(z) = \begin{cases} s_1\phi & 0 \leq z \leq z_1, \\ 0 & z_1 < z \leq z_2, \\ -s_2\phi & z_2 < z \leq z_3, \end{cases} \tag{7}$$

where s_1 is the proliferation rate in the SB and s_2 is the disintegration rate in SG, both assumed constant. Combining this form of $f(z)$ with considerations from previous sections yields

$$u_i(z) = \begin{cases} s_1 z & 0 \leq z \leq z_1, \\ s_1 z_1 & z_1 \leq z \leq z_2, \\ s_1 z_1 - s_2(z - z_2) & z_2 \leq z \leq z_3, \end{cases} \tag{8a}$$

$$u_e(z) = \begin{cases} \phi\left(s_1(z_1 - z) - s_2(z_3 - z_2)\right)/(1-\phi) & 0 \leq z \leq z_1, \\ -s_2\phi(z_3 - z_2)/(1-\phi) & z_1 \leq z \leq z_2, \\ -s_2\phi(z_3 - z)/(1-\phi) & z_2 \leq z \leq z_3, \end{cases} \tag{8b}$$

Parameter		Value	References
Diffusion coefficient of calcium in viable epidermal ECF	D	$1 \times 10^{-9}\,\mathrm{m}^2\,\mathrm{sec}^{-1}$	[44–46]
Cell volume fraction in viable epidermis	ϕ	0.96 ± 0.03	[22, 47]
Proliferation rate in the SB	s_1	$2.7 \times 10^{-6}\,\mathrm{sec}^{-1}$	[48]
Total volume reduction of a keratinocyte during its passage through the SG	R	0.46 ± 10	[49]
Viable sublayer heights above the BM for human epidermis	z_1	$28 \pm 17\,\mu\mathrm{m}$	[4, 12, 50]
	z_2	$83 \pm 20\,\mu\mathrm{m}$	[4, 12, 50]
	z_3	$115 \pm 3\,\mu\mathrm{m}$	[12, 50]
Viable sublayer heights above the BM for murine epidermis	z_1	$20\,\mu\mathrm{m}$	[24]
	z_2	$60\,\mu\mathrm{m}$	[24]
	z_3	$90\,\mu\mathrm{m}$	[24]

Table 1: Parameter values used in numerical solutions throughout this paper. Justification is provided in Appendix A.

thereby giving expressions for the cell and ECF velocities in the viable epidermis.

For equations (8a) and (8b) to be physically reasonable requires that the inequality

$$s_1 > \frac{s_2(z_3 - z_2)}{z_1}, \tag{9}$$

is satisfied. This inequality ensures that the cell velocity at the SG-SC interface is positive, so that SC is produced. The disintegration rate s_2 is written in terms of the total volume reduction R of a keratinocyte due to disintegration during its passage through the SG, and is given by

$$s_2 = \frac{Rs_1z_1}{z_3 - z_2}, \tag{10}$$

where the derivation of this equation is given in Appendix B.

A profile of cell and ECF velocities in human epidermis, produced using equations (8a), (8b) and (10), is presented in Figure 3. The parameters used are given in Table 1, with justification for these parameters provided in Appendix A.

3.2. Physical interpretation of the cell and fluid velocities

The forms of the cell and ECF velocities in Figure 3 are relatively intuitive. In the SB, the cell velocity increases linearly from zero due to the proliferation occurring constantly throughout this sublayer. Simultaneously, the ECF velocity decreases linearly to satisfy mass conservation of the fluid. The positive ECF velocity at the BM follows from inequality (9), whilst the negative ECF

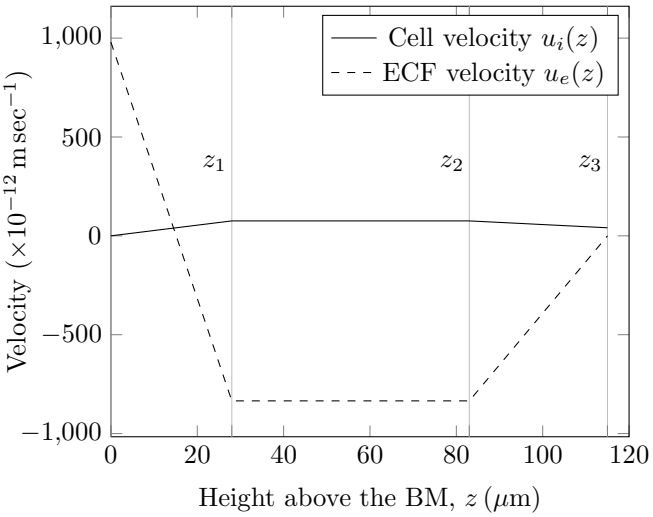

Figure 3: The physical cell and ECF velocities in the viable epidermal sublayers, calculated using equations (8a), (8b) and (10) from mean values of the parameters for human epidermis shown in Table 1.

velocity at the SB-SS interface occurs because the cellular fluid expelled during disintegration in the SG travels towards the BM to construct daughter cells in the SB.

In the SS, the cell and ECF velocities are constant because $f = 0$ in this sublayer. The cell velocity is positive because keratinocytes are migrating passively towards the skin surface, and the ECF velocity is negative because this fluid is travelling towards the BM as previously described.

In the SG, the cell velocity decreases linearly due to the constant disintegration throughout this layer. The cell velocity at the SG-SC interface is positive so that SC is produced, corresponding to inequality (9). Simultaneously, the negative ECF velocity decreases linearly in magnitude to zero at the SG-SC interface so that no ECF enters the SC.

The cell velocity distribution can be used to predict transit times τ_j through each epidermal sublayer j according to

$$\tau_j = \int_{z_{j-1}}^{z_j} \frac{dz}{u_i(z)}, \qquad j = 1, 2, 3, \tag{11}$$

where τ_1, τ_2 and τ_3 correspond to transit times through the SB, SS and SG respectively. τ_1 cannot be calculated because $u_i(0) = 0$ yields a singularity in its expression; physically, this occurs because stem cells are not considered in our model. From calculation of τ_2 and τ_3 using parameter values from Table 1 substituted into equation (11), we predict transit times through viable human epidermis of at least 14-18 days. The experimental transit time through viable murine epidermis is 4-7 days [51], whilst viable human epidermis estimates vary

from 10-14 days [52] to 38-61 days [53]. Thus, the cell velocities predicted by our model agree with experimental data for cell transit times, especially [53].

3.3. Regulation of the extracellular calcium profile

Previously, Cornelissen *et al.* [23] used a mathematical model to conclude that electrophoresis is the main mechanism regulating the free calcium profile. Their simulation profile is nearly constant in the viable sublayers, a result also obtainable if diffusion is the dominant mechanism. Similarly, we investigate the hypothesis that the extracellular calcium profile can be regulated primarily by diffusion.

The extracellular calcium flux is assumed to consist of two contributions: advection matching the ECF velocity and Fickian diffusion with constant coefficient D,

$$\rho_{ce}(z)u_{ce}(z) = \rho_{ce}(z)u_e(z) - D\frac{\mathrm{d}\rho_{ce}(z)}{\mathrm{d}z}. \tag{12}$$

We demonstrate that the advection is negligible compared to diffusion, by considering the sublayer where advection is strongest: the SS. Equations (8b), (10) and (12) are combined to obtain, in the SS,

$$\rho_{ce}(z)u_{ce}(z) = -\left(\frac{Rs_1z_1\phi}{1-\phi}\rho_{ce}(z) + D\frac{\mathrm{d}\rho_{ce}(z)}{\mathrm{d}z}\right). \tag{13}$$

We temporarily introduce the dimensionless variables

$$u^*_{ce} = \frac{u_{ce}\hat{t}}{\hat{z}}, \quad z^* = \frac{z}{\hat{z}}, \quad \text{where} \quad \hat{z} = z_1, \quad \hat{t} = \frac{z_1^2}{D}, \tag{14}$$

and substitute these variables into (13), obtaining

$$\rho_{ce}(z)u^*_{ce}(z) = -\left(\mathrm{Pe}\,\rho_{ce}(z) + \frac{\mathrm{d}\rho_{ce}(z)}{\mathrm{d}z^*}\right), \tag{15}$$

where the Péclet number, Pe, represents the strength of advection compared to diffusion,

$$\mathrm{Pe} = \frac{Rs_1z_1^2\phi}{(1-\phi)} \,/\, D, \tag{16}$$

with advective and diffusive contributions to the Péclet number separated by the solidus. Substitution of parameter values from Table 1 into equation (16) yields an advective contribution of $\mathcal{O}(10^{-14}\,\mathrm{m^2\,sec^{-1}})$, diffusive contribution of $D = 10^{-9}\,\mathrm{m^2\,sec^{-1}}$, and hence Péclet numbers of $\mathcal{O}(10^{-5})$. Thus, advection is negligible compared to diffusion.

In preliminary simulations we determined that the calcium influx $g(z)$ is negligible compared to the extracellular diffusion (data not shown). We will not prove this directly, but make use of this simplification and show later in our results (Section 3.5) that it is in fact true.

From the above considerations, equation (1d) simplifies to

$$D\frac{\mathrm{d}^2\rho_{ce}(z)}{\mathrm{d}z^2} = 0 \tag{17}$$

and combining with boundary conditions (4) and (6) yields

$$\rho_{ce}(z) = \rho_0, \qquad 0 \le z \le z_3. \tag{18}$$

Hence, a constant extracellular calcium profile in the viable sublayers can result from regulation by diffusion. This result implies that the intracellular calcium is the source of the shape of the total epidermal calcium profile, and that the calcium exchanges between the keratinocytes and ECF must vary with height above the BM to give rise to this shape. Thus, in addition to passive regulation, the calcium profile is actively regulated by the differences in these exchanges. In the next section we will determine these calcium exchange profiles $g(z)$.

3.4. Calcium exchange profiles

Calcium exchange profiles can be obtained from calcium profiles using the following three-step process:

1. The intracellular calcium profile $\rho_{ci}(z)$ in the viable epidermis is obtained from the experimental total calcium profile $\rho(z)$ according to

$$\rho_{ci}(z) = \rho(z) - (1-\phi)\rho(0), \qquad 0 \le z \le z_3. \tag{19}$$

   This equation is derived in Appendix C.
2. The cell velocity profile $u_i(z)$ in the viable epidermis is determined by

$$u_i(z) = \begin{cases} s_1 z & 0 \le z \le z_1, \\ s_1 z_1 & z_1 \le z \le z_2, \\ s_1 z_1 \left(1 - R(z-z_2)/(z_3-z_2)\right) & z_2 \le z \le z_3. \end{cases} \tag{20}$$

   This equation follows from combination of (8a) and (10).
3. The calcium exchange profile $g(z)$ is then determined using equation (1c),

$$g(z) = \frac{\mathrm{d}}{\mathrm{d}z}\left(\rho_{ci}(z)u_i(z)\right), \qquad 0 \le z \le z_3.$$

We applied this three-step process to two experimental calcium profiles: a human epidermis profile shown in Figure 4a [12] and a murine epidermis profile shown in Figure 4b [24]. The differentiation in Step 3 was performed using a numerical three-point finite difference scheme.

The calcium transfer profiles obtained are shown in Figures 4c and 4d for human and murine epidermis respectively. In human epidermis, the calcium influx is relatively constant in the SB and SS, peaking slightly in the SG before rapidly reversing direction to outflux. The uncertainty is small in the SB and SS, but increases in the SG due to the increased uncertainty of $\rho(z)$ in this

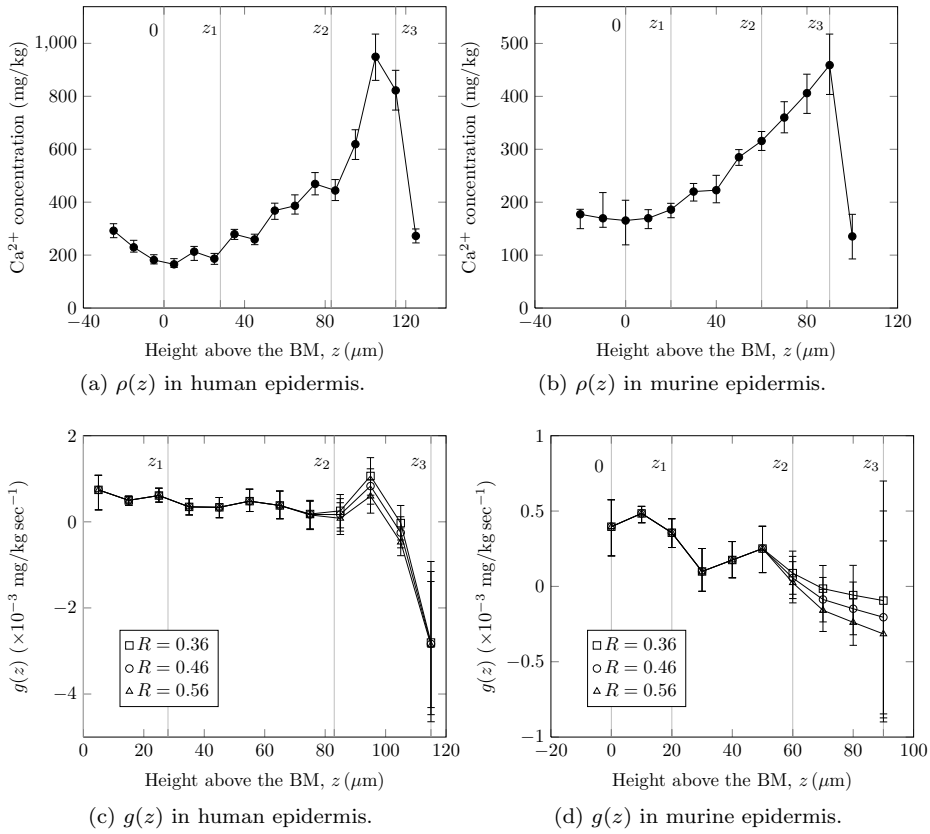

(a) $\rho(z)$ in human epidermis.

(b) $\rho(z)$ in murine epidermis.

(c) $g(z)$ in human epidermis.

(d) $g(z)$ in murine epidermis.

Figure 4: Experimental calcium profiles $\rho(z)$ in human epidermis (a) and murine epidermis (b), and cellular calcium transfer rates $g(z)$ in (c) and (d) predicted from these profiles using our model. The calcium profiles are reproduced from [12] (human, a) and [24] (murine, b) using xyExtract V3.1 (2008). The calcium transfer rates (c, d) are calculated by use of equations (19), (20) and (1c) and parameters $\phi = 0.96 \pm 0.03$ and the mean values of s_1, z_1, z_2, z_3 from Table 1. The uncertainties in (c, d) arise from the uncertainties in $\rho(z)$ and ϕ.

sublayer (see Figure 4a). In murine epidermis, the calcium exchange profile is less distinctive, with influx in the SB and SS and outflux in the SG. Hence for both human and murine epidermis, keratinocytes switch from calcium influx to outflux during progression from the SS to the SG, and this switch actively regulates the epidermal calcium profile in both species.

As can be seen in Figures 4c and 4d, the results are relatively insensitive to the uncertainties in ϕ and R. For human epidermis, the uncertainty in parameters z_1 and z_2 affects the transfer profile in the following ways (data not shown). Small z_1 yields a smaller plateau $g(z)$ value in the SB and SS (three- to five-fold difference between lower and upper limits of z_1), and an additional peak in the SB which is an artefact attributable to the change in gradient of $u_i(z)$ at z_1. Small z_2 yields a thinner $g(z)$ plateau region, and an additional trough in the SG just prior to the peak at $z \approx 95\,\mu$m. The influx peak at $z \approx 95\,\mu$m occurs regardless of the choice of parameters.

The calcium exchange profiles allow investigation of whether or not the high calcium outflux in the SG requires cellular breakdown. Murine keratinocytes *in vitro* can remove $^{45}Ca^{2+}$ from the ECF at a rate of $2\,\text{nmol}/10^6$ cells/min [54], which corresponds to $2 \times 10^{-3}\,\text{mg/kg}\,\text{sec}^{-1}$. This value is above the upper limit of $|g(z)|$ for murine epidermis (see Figure 4d). Hence, the calcium outflux in the SG predicted by our model can occur whilst the keratinocyte cellular membrane is intact.

3.5. Calcium influx negligibly affects the extracellular calcium profile

Finally, we show that $g(z)$ has negligible effect on the extracellular calcium distribution. This was an essential assumption for the derivations presented in Section 3.3. Let us assume that $g(z)$ is non-negligible, modifying equation (17) to

$$0 = D\frac{\mathrm{d}^2\rho_{ce}(z)}{\mathrm{d}z^2} - g(z), \tag{21}$$

and constant and equal to g_1 throughout the viable epidermis. This yields a solution of (21), with boundary conditions (4) and (6), of

$$\rho_{ce}(z) = \rho_0 + \frac{g_1 z}{2D}(z - 2z_3). \tag{22}$$

In the domain $z \in [0, z_3]$ of our model, this equation gives that the maximum difference between $\rho_{ce}(z)$ and $\rho_{ce}(0) = \rho_0$ occurs when $z = z_3$. When taking into account the uncertainties in all parameters in Table 1, we found an upper limit for $|g(z)|$ of $0.015\,\text{mg/kg}\,\text{sec}^{-1}$ in viable epidermis for humans and mice (data not shown). Thus, using equation (22) to evaluate $|\rho_{ce}(z_3) - \rho_{ce}(0)|$ with g_1 set to this upper bound on the magnitude of $g(z)$, determines the upper bound on the variation that this $g(z)$ can provide to the $\rho_{ce}(z)$ distribution across the entire domain $[0, z_3]$ of our model.

Equation (22), evaluated with $g_1 = 0.015\,\text{mg/kg}\,\text{sec}^{-1}$ and the values of D and maximum z_3 substituted from Table 1, yields $|\rho_{ce}(z_3) - \rho_{ce}(0)| \approx 0.1\,\text{mg/kg}$. This value is insignificant compared to the experimental calcium profiles. Because a constant $g(z) = g_1$ that possesses higher magnitude than all predicted

values of $g(z)$ in human or murine epidermis yields negligible variation of $\rho_{ce}(z)$, we confirm that $\rho_{ce}(z)$ is essentially constant and that $g(z)$ has negligible effect on the extracellular calcium distribution.

4. Discussion

Our theoretical work contributes to the discussion [20, 22] of the role of active and passive mechanisms in the regulation of the epidermal calcium profile. It is already clear that this profile is passively regulated by the impermeable barrier of the SC, as the absence of this barrier leads to calcium deposition in this sublayer, as observed in *in vitro* reconstructed epidermis [16]. Further, Elias *et al.* have argued that passive processes alone can be responsible for regulation of the calcium profile [20].

Hence we assumed that the calcium profile is passively regulated by the impermeable barrier of the SC, by use of boundary condition (6). We found that diffusion governs extracellular calcium motion in the viable epidermis and hence the extracellular calcium profile is constant (see Section 3.3). This in turn indicates that intracellular calcium is the main source of the calcium profile, which agrees with the recent localisation of the bulk of free epidermal calcium to intracellular stores such as the endoplasmic reticulum and Golgi apparatus [22], and observations in other cell types of higher calcium concentrations in the endoplasmic reticulum ($5 - 50\,\mathrm{mM}$) [55] than in the ECF ($\sim 2\,\mathrm{mM}$) [17].

Combining these results with experimental data for the total calcium profile, we determined the pattern of calcium exchange between keratinocytes and ECF in the viable epidermis (see Section 3.4). We found that, in both human and murine epidermis, there is influx of calcium ions into keratinocytes in the SB and SS, and outflux of these ions in the SG. Calcium pumps present on keratinocyte cellular membranes are likely to be responsible for the calcium exchange between keratinocytes and the ECF. The importance of these keratinocyte pumps in maintaining healthy epidermis is shown by the recent association of mutations in these pumps with the skin lesions of Hailey-Hailey and Darier diseases [56]. The differences in the actions of these pumps in the SG and underlying sublayers represent an active regulation of the intracellular calcium profile, which we have already suggested is the main source of the total calcium profile. Hence our work suggests that the epidermal calcium profile is actively regulated [22] by the calcium influx and outflux in the different epidermal sublayers, in addition to its passive regulation by the impermeable barrier of the SC.

Further to our argument, wounding the epidermis obliterates its calcium profile, due in part to the disappearance of calcium from the cytosol of keratinocytes in the SG [21]. Increased calcium outflux in the SG, promoted by membrane pumps in the presence of wounding, may explain this disappearance. Because the calcium profile re-establishes gradually with the permeability barrier [21], we suggest that the active regulation of the epidermal calcium profile by keratinocyte membrane calcium pumps extends to the ability of the epidermis to re-establish normal function after injury.

The peak in $g(z)$ prior to rapid cellular calcium expulsion in human epidermis (see Figure 4c) could be interpreted as an indication of keratinocyte membrane dysfunction early during disintegration. In order for keratinocytes to expel their calcium in the SG, they must first release the calcium sequestered in intracellular stores [22]. This causes a temporary sharp increase in cytosolic calcium during disintegration which has been experimentally observed in the SG [1, 16]. The peak of $g(z)$ prior to calcium expulsion could represent a contribution from the ECF to this cytosolic calcium increase, due to some dysfunction of the cell membrane. This possible early disintegration event also fits with the observation [57] of decreasing expression and enzymatic activity of calcium membrane pumps with differentation state. On the other hand, we calculated that it is possible for the high calcium outflux in the SG to occur while the cellular membrane is still intact (see Section 3.4).

We found a constant extracellular calcium profile, but this profile is reported to vary with epidermal sublayer [1]. Whilst the shape of this profile has only been reported semi-quantitatively and varies with species and publication, the general trend [1, 16, 58] is a relatively constant concentration in the SB and SS, a slight increase in the SG and a sharp drop in the SC. The only disagreement between our work and this extracellular profile is the slightly increased calcium concentration in the SG. The discrepancy could be attributed to decreased diffusion coefficient in the SG caused by the increased presence of extracellular lipids [59] or tight junctions [60]. However, variations in the extracellular calcium profile should not significantly affect our results because of the small volume of the ECF occupied by this calcium ($\leq 7\%$) [22, 47].

Our model did not account for stem cells, but the separation of the SB into stem cell and transit-amplifying cell subpopulations explains a mathematical singularity present at the BM in our model construction. In the SB, stem cells divide indefinitely, each time producing transit-amplifying cells. These transit-amplifying cells divide only a few times before leaving the SB [61]. In the current form of our model, $u_i(0) = 0$ makes the transit time through the SB infinite. Also, equation (19) indicates that $\rho_{ci}(0) > 0$, which together with our assumption that intracellular calcium cannot travel across the BM in boundary condition (3), implies a singularity in calcium influx at the BM. Both these issues of the model can be resolved by including stem cells. If stem cells are assumed present on the BM, they may possess a relatively constant intracellular calcium reservoir that explains the positive $\rho_{ci}(0)$ seen here. Also, because stem cells are dividing indefinitely, we can separate their infinite transit time from the finite transit time of their offspring, transit-amplifying cells. These stem cells should not otherwise affect the results presented here, because as previously stated they account for only 1-10% of the SB [42].

We found that cellular calcium influx is positive throughout the SB and SS, and possibly constant in human epidermis (see Figures 4c and 4d). This description of cellular calcium transfer is different from those assumed by previous mathematical models. The agent-based simulation of epidermis by Grabe and Neuber [25] assumed that calcium is only taken in by cells in the SB, whilst Cornelissen *et al.* [23] assumed a rather complex form of calcium transfer between

free and bound states. The unreproducibility of the constant calcium influx in murine epidermis that we observed could be attributed to the resolution of the experimental technique (PIXE, $\sim 10\,\mu$m) used to obtain the experimental calcium profiles [62]. Alternatively, it could be a species difference: murine epidermis [33] is thinner and contains fewer cell layers than human epidermis [4], and so may contain differences in the regulation of its homeostasis.

The model can be extended to: (1) investigate the extracellular calcium gradient, (2) include additional sublayers such as the stem and transit-amplifying cell populations and the lower SC, (3) use separate equations for intracellular calcium present in the cytosol and organelles, (4) include keratinocyte size variation prior to disintegration, (5) include lipids as a second species, and (6) include time-dependence of epidermal sublayer thicknesses based on the calcium transfer profiles identified here for investigation of wounding and recovery [20], skin diseases such as psoriasis [63] and the short lifespan of epidermal substitutes [64]. Regardless of the future direction, the complexity of epidermal calcium dynamics ensure that it is an interesting problem for future experimental and theoretical research.

5. Acknowledgements

The corresponding author wishes to thank the Institute of Health and Biomedical Innovation, Queensland University of Technology, for their financial support for this work. This research was undertaken as part of the Australian Research Council (ARC) Discovery Grant DP0773230.

Appendix A. Parameters

Table 1 lists parameters used in this paper and their key references. Here, we present the justification of the parameter values, starting from the experimental literature and applying subsequent calculations where necessary.

Appendix A.1. Diffusion coefficient of calcium in viable epidermal ECF, D

The ECF is essentially water [65]. Thus, we assume that the diffusion coefficient of calcium in the ECF, D, is equal to that of calcium ions in water at skin temperature. In the temperature range 0-100°C, dependence of D on temperature adheres well to the Stokes-Einstein equation [44],

$$\left(\frac{D^0\eta^0}{T}\right)\Big|_{T_1} = \left(\frac{D^0\eta^0}{T}\right)\Big|_{T_2}, \tag{A.1}$$

where D^0 is the diffusion coefficient of a compound in water at infinite dilution, η^0 is the water viscosity, and T is the absolute temperature.

We use the Stokes-Einstein equation to estimate the diffusion coefficient of calcium ions in water at skin temperature, and hence the physical diffusion coefficient of calcium in the viable mammalian epidermal ECF, from: (1) the

diffusion coefficient of calcium ions in water at infinite dilution and 0°C [44], (2) an average skin temperature of 35°C [45], and (3) water viscosity values at 0°C and 35°C reported in [46].

Appendix A.2. Cell volume fraction in viable epidermis, ϕ

Elias and Leventhal [47] reported $\phi = 0.990$-0.995 in the SG of murine epidermis, whilst Celli *et al.* [22] reported that ϕ increases from 0.93 in the SB to 0.98 in the SG in humans. We combine these values to choose $\phi = 0.96 \pm 0.03$.

Appendix A.3. Proliferation rate in the SB, s_1

Castelijns *et al.* [48] reported that the cell cycle time in human epidermis is $\sim$62.5 hours. The cell cycle time can be inverted to obtain a proliferation rate of $4.4 \times 10^{-6}\,\mathrm{sec}^{-1}$. However, the growth fraction in the SB is only 60% [66, 67], resulting in an adjustment to the proliferation rate to $s_1 = 2.7 \times 10^{-6}\,\mathrm{sec}^{-1}$, which is the value we use for both human and murine epidermis in this paper.

However, estimates of proliferation rates vary by up to an order of magnitude. Potten [66] reported that the dorsum and ear of murine epidermis possesses a proliferation rate of ~ 0.7 cells/100 basal cells/hour, which corresponds to $s_1 = 1.9 \times 10^{-6}\,\mathrm{sec}^{-1}$. On the other hand, Iizuka [67] reported that there are 27,000 cells and a birth rate of 1,246 cells per day in a $1\,\mathrm{mm}^2$ section of the proliferative compartment of the epidermis [67]. Dividing the birth rate by the number of cells yields $s_1 = 5.3 \times 10^{-7}\,\mathrm{sec}^{-1}$.

Regardless, in our model s_1 affects the magnitude but not the shape of calcium transfer profiles $g(z)$, as these profiles scale linearly with the value of s_1. This can be seen from equations (1c) and (20), if they are rewritten as

$$g(z) = s_1 \frac{\mathrm{d}}{\mathrm{d}z}\left(\rho_{ci}(z) u_i^*(z)\right),$$
$$u_i^*(z) = \begin{cases} z & 0 \le z \le z_1, \\ z_1 & z_1 \le z \le z_2, \\ z_1\left(1 - R(z - z_2)/(z_3 - z_2)\right) & z_2 \le z \le z_3, \end{cases} \tag{A.2}$$

where $u_i^*(z) = u_i(z)/s_1$.

Appendix A.4. Total volume reduction of a keratinocyte during its passage through the SG, R

Norlén and Al-Amoudi [49] reported that the volumes of viable keratinocytes and corneocytes are $700-900\,\mu\mathrm{m}^3$ and $400-450\,\mu\mathrm{m}^3$ respectively, corresponding to a volume reduction of $R = 0.46 \pm 0.10$.

Appendix A.5. Viable sublayer heights above the BM, z_1, z_2 and z_3

For the human epidermal calcium profile investigated, the total epidermis thickness of $125\,\mu\mathrm{m}$ is provided [12]. To estimate z_1, z_2 and z_3, we use other literature sources. First, the thickness of human SC is $\sim 10 \pm 3\,\mu\mathrm{m}$ [50], so

$z_3 = 115 \pm 3\,\mu$m. Second, the typical number of cell layers in the SB, SS and SG are used to estimate z_1 and z_2, as described in the following paragraph.

Forslind and Lindberg [4] report that the SB contains 1-2 cell layers, the SS contains 2-7 cell layers, and the SG contains 2-3 cell layers. We assume that keratinocytes change little in size during passage through the viable epidermis, except in the SG. Thus, the SG is the only epidermal sublayer where the cell layers have different thicknesses. Because SG keratinocytes lose $(46 \pm 10)\%$ of their volume [49], and this loss is linear as a function of height above the SS-SG boundary, the average volume of SG keratinocytes is $((100\% - (46 \pm 10)\%) + 100\%)/2 = (72 \pm 5)\%$ of the volume of SB and SS keratinocytes. Thus, the SG contains the equivalent of 1.3-2.3 layers of non-disintegrated cells. Combining this information with the previously stated number of cell layers for the SB and SS from [4] and the previously calculated value of $z_3 = 115 \pm 3\,\mu$m [12, 50], yields $z_1 = 28 \pm 17\,\mu$m and $z_2 = 83 \pm 20\,\mu$m.

For the murine epidermal calcium profile investigated, the viable epidermal sublayer heights are provided [24]: $z_1 = 20\,\mu$m, $z_2 = 60\,\mu$m and $z_3 = 90\,\mu$m.

Appendix B. Disintegration rate s_2 in terms of cell volume loss R

Equation (10) in Section 3.1 expresses the disintegration rate s_2 in terms of the total volume reduction R of a keratinocyte due to disintegration during its passage through the SG. Here, we provide the derivation of this equation.

The time τ_3 taken for a cell to travel through the SG can be determined using equation (11). Substitution of equation (8a) into (11) for the SG, and subsequent integration and rearrangement yields

$$1 - \exp\left(-s_2\tau_3\right) = \frac{s_2(z_3 - z_2)}{s_1 z_1}. \tag{B.1}$$

In the SG, the cell volume fraction ϕ is reduced by $g(z) = -s_2\phi$, which corresponds to cell disintegration proportional to ϕ with constant s_2. We consider the rate of change of volume $V(t)$ of a single keratinocyte as it passively migrates through the SG. This keratinocyte's volume reduction $\mathrm{d}V/\mathrm{d}t$ is similarly proportional to $V(t)$ with constant s_2,

$$\frac{\mathrm{d}V}{\mathrm{d}t} = -s_2 V(t), \tag{B.2}$$

which can be solved to give

$$V(t) = V(0)\exp\left(-s_2 t\right), \tag{B.3}$$

where $V(0)$ is the keratinocyte's volume at z_2. We define R as the total volume reduction of a keratinocyte during its passage through the SG, in terms of the keratinocyte volumes $V(0)$ at z_2 and $V(\tau_3)$ at z_3 giving

$$R = 1 - \frac{V(\tau_3)}{V(0)}. \tag{B.4}$$

Substitution of expressions for $V(t)$ from equation (B.3) into (B.4) yields

$$R = 1 - \exp\left(-s_2\tau_3\right). \tag{B.5}$$

Comparison of equations (B.1) and (B.5) immediately gives

$$R = \frac{s_2(z_3 - z_2)}{s_1 z_1}. \tag{B.6}$$

Rearranging this equation for s_2 immediately yields the desired equation (10).

Appendix C. Intracellular calcium $\rho_{ci}(z)$ in terms of total calcium $\rho(z)$

Equation (19) in Section 3.4 expresses the intracellular calcium $\rho_{ci}(z)$ in terms of the total calcium $\rho(z)$. Here, we provide the derivation of this equation.

Experimental calcium profiles $\rho_{ci}(z)$ consist of intracellular and extracellular localisations,

$$\begin{aligned}\rho(z) &= \rho_{ci}(z) + \rho_{ce}(z)\\ &= \rho_{ci}(z) + \rho_0,\end{aligned} \tag{C.1}$$

the latter equation following from (18). Although the total calcium profile across the BM is continuous (see Figures 4a and 4b), the free calcium concentration in the dermis is significantly higher than in the SB [22]. We assume that all calcium in the upper dermis can freely move throughout it in a similar fashion to the epidermal extracellular calcium in our model.

Recall boundary condition (3), which states that intracellular calcium cannot travel across the BM because it is stored within keratinocytes. This implies that motion of calcium across the BM only involves transfer between the free dermal and extracellular epidermal calcium. We assume that the BM provides no barrier for this transfer. Thus, these concentrations must match at the BM for continuity. That is

$$\rho(0) = \frac{\rho_{ce}(0)}{1 - \phi(0)}. \tag{C.2}$$

Combining equations (18) and (C.1) gives

$$\rho_0 = (1 - \phi)\rho(0) \tag{C.3}$$

and substitution into (C.2) immediately yields the desired equation (19).

References

[1] G. Menon, S. Grayson, P. Elias, Ionic calcium reservoirs in mammalian epidermis: ultrastructural localization by ion-capture cytochemistry, J. Invest. Dermatol. 84 (1985) 508–512.

[2] H. Hennings, D. Michael, C. Cheng, P. Steinert, K. Holbrook, S. Yuspa, Calcium regulation of growth and differentiation of mouse epidermal cells in culture, Cell 19 (1980) 245–254.

[3] E. Houben, K. D. Paepe, V. Rogiers, A keratinocyte's course of life, Skin Pharmacol. Physiol. 20 (2007) 122–132.

[4] B. Forslind, M. Lindberg (Eds.), Skin, hair, and nails: structure and function, Marcel Dekker, New York, 2004.

[5] R. Wickett, M. Visscher, Structure and function of the epidermal barrier, Am. J. Infect. Control 34 (2006) S98–S110.

[6] P. Elias, K. Feingold (Eds.), Skin barrier, Taylor and Francis, New York, 2006.

[7] J. Waller, H. Maibach, Age and skin structure and function, a quantitative approach (I): blood flow, pH, thickness, and ultrasound echogenicity, Skin Res. Technol. 11 (2005) 221–235.

[8] E. Fuchs, S. Raghavan, Getting under the skin of epidermal morphogenesis, Nat. Rev. Genet. 3 (2002) 199–209.

[9] J. Whitfield, B. Chakravarthy, Calcium: the grand-master cell signaler, National Research Council Research Press, Ottawa, Canada, 2001.

[10] M. Falcke, Reading the patterns in living cells - the physics of Ca^{2+} signaling, Adv. Phys. 53 (2004) 225–440.

[11] J. Keener, J. Sneyd, Mathematical physiology. I: Cellular physiology, 2nd Edition, Interdisciplinary Applied Mathematics 8/1, Springer, New York, 2009.

[12] M. Behne, C.-L. Tu, I. Aronchik, E. Epstein, G. Bench, D. Bikle, T. Pozzan, T. Mauro, Human keratinocyte ATP2C1 localizes to the Golgi Ca^{2+} stores, J. Invest. Dermatol. 121 (2003) 688–694.

[13] M. Berridge, M. Bootman, H. Roderick, Calcium signalling: dynamics, homeostasis and remodelling, Nat. Rev. Mol. Cell Biol. 4 (2003) 517–529.

[14] M. Berridge, The endoplasmic reticulum: a multifunctional signaling organelle, Cell Calcium 32 (2002) 235–249.

[15] K. V. Baelen, L. Dode, J. Vaoevelen, G. Callewaert, H. D. Smedt, L. Missiaen, J. Parys, L. Raeymaekers, F. Wuytack, The Ca^{2+}/Mn^{2+} pumps in the Golgi apparatus, Biochim. Biophys. Acta 1742 (2004) 103–112.

[16] J. Vičanová, E. Boelsma, A. Mommaas, J. Kempenaar, B. Forslind, J. Pallon, T. Egelrud, H. Koerten, M. Ponec, Normalization of epidermal calcium distribution profile in reconstructed human epidermis is related to improvement of terminal differentiation and stratum corneum barrier formation, J. Invest. Dermatol. 111 (1998) 97–106.

[17] D. Clapham, Calcium signaling, Cell 131 (2007) 1047–1058.

[18] J. Meldolesi, F. Grohovaz, Total calcium ultrastructure: advances in excitable cells, Cell Calcium 30 (2001) 1–8.

[19] M. Brini, E. Carafoli, Calcium pumps in health and disease, Physiol. Rev. 89 (2009) 1341–1378.

[20] P. Elias, S. Ahn, B. Brown, D. Crumrine, K. Feingold, Origin of the epidermal calcium gradient: regulation by barrier status and role of active *vs* passive mechanisms, J. Invest. Dermatol. 119 (2002) 1269–1274.

[21] G. Menon, P. Elias, S. Lee, K. Feingold, Localization of calcium in murine epidermis following disruption and repair of the permeability barrier, Cell Tissue Res. 270 (1992) 503–512.

[22] A. Celli, S. Sanchez, M. Behne, T. Hazlett, E. Gratton, T. Mauro, The epidermal Ca^{2+} gradient: measurement using the phasor representation of fluorescent lifetime imaging, Biophys. J. 98 (2010) 911–921.

[23] L. Cornelissen, C. Oomens, J. Huyghe, F. Baaijens, Mechanisms that play a role in the maintenance of the calcium gradient in the epidermis, Skin Res. Technol. 13 (2007) 369–376.

[24] T. Mauro, G. Bench, E. Sidderas-Haddad, K. Feingold, P. Elias, C. Cullander, Acute barrier perturbation abolishes the Ca^{2+} and K^{+} gradients in murine epidermis: quantitative measurement using PIXE, J. Invest. Dermatol. 111 (1998) 1198–1201.

[25] N. Grabe, K. Neuber, A multicellular systems biology model predicts epidermal morphology, kinetics and Ca^{2+} flow, Bioinformatics 21 (2005) 3541–3547.

[26] C. Please, G. Pettet, D. McElwain, A new approach to modelling the formation of necrotic regions in tumours, Appl. Math. Lett. 11 (1998) 89–94.

[27] A.-R. Khaled, K. Vafai, The role of porous media in modeling flow and heat transfer in biological tissues, Int. J. Heat Mass. Tran. 46 (2003) 4989–5003.

[28] K. Khanafer, K. Vafai, The role of porous media in biomedical engineering as reltaed to magnetic resonance imaging and drug delivery, Heat Mass Transfer 42 (2006) 939–953.

[29] A. Datta, Porous media approaches to studying simultaneous heat and mass transfer in food processes. I: Problem formulations, J. Food Eng. 80 (2007) 80–95.

[30] Y.-L. Chuang, R. Oren, A. Bertozzi, N. Phillips, G. Katul, The porous media model for the hydraulic system of a conifer tree: Linking sap flux data to transpiration rate, Ecol. Model. 191 (2006) 447–468.

[31] J. Fozard, H. Byrne, O. Jensen, J. King, Continuum approximations of individual-based models for epithelial monolayers, Math. Med. Biol. 27 (2010) 39–74.

[32] J. Hanson, The histogenesis of the epidermis in the rat and mouse, J. Anat. 81 (1947) 174–197.

[33] T. Allen, C. Potten, Ultrastructural site variations in mouse epidermal organization, J. Cell Sci. 21 (1976) 341–359.

[34] M. Tsutsumi, K. Inoue, S. Denda, K. Ikeyama, M. Goto, M. Denda, Mechanical-stimulation-evoked calcium waves in proliferating and differentiated human keratinocytes, Cell Tissue Res. 338 (2009) 99–106.

[35] T. Roose, S. Chapman, P. Maini, Mathematical models of avascular tumor growth, SIAM Rev. 49 (2007) 179–208.

[36] J. P. D. Plessis (Ed.), Fluid transport in porous media, Advances in Fluid Mechanics 13, Computational Mechanics Publications, Southampton, UK, 1997.

[37] A. Gandolfi, M. Iannelli, G. Marinoschi, An age-structured model of epidermis growth, J. Math Biol. 62 (2011) 111–141.

[38] G. Menon, P. Elias, K. Feingold, Integrity of the permeability barrier is crucial for maintenance of the epidermal calcium gradient, Br. J. Dermatol. 130 (1994) 139–147.

[39] I. Blank, J. M. III, A. Emslie, I. Simon, C. Apt, The diffusion of water across the stratum corneum as a function of its water content, J. Invest. Dermatol. 82 (1984) 188–194.

[40] E. Fuchs, Epidermal differentiation: the bare essentials, J. Cell Biol. 111 (1990) 2807–2814.

[41] F. Watt, Stem cell fate and patterning in mammalian epidermis, Curr. Opin. Genet. Dev. 11 (2001) 410–417.

[42] A. Li, P. Simmons, P. Kaur, Identification and isolation of candidate human keratinocyte stem cells based on cell surface phenotype, P. Natl. Acad. Sci. USA 85 (1998) 3902–3907.

[43] P. Corcuff, C. Bertrand, J. Leveque, Morphometry of human epidermis *in vivo* by real-time confocal microscopy, Arch. Dermatol. Res. 285 (1993) 475–481.

[44] Y.-H. Li, S. Gregory, Diffusion of ions in sea water and in deep-sea sediments, Geochim. Cosmochim. Ac. 38 (1974) 703–714.

[45] E. Williams, A. Heusch, P. McCarthy, Thermal screening of facial skin arterial hot spots using non-contact infrared radiometry, Physiol. Meas. 29 (2008) 341–348.

[46] P. Kampmeyer, The temperature dependence of viscosity for water and mercury, J. Appl. Phys. 23 (1952) 99–102.

[47] P. Elias, M. Leventhal, Intercellular volume changes and cell surface expansion during cornification, Clin. Res. 27 (1979) 525A.

[48] F. Castelijns, J. Ezendam, M. Latijnhouwers, I. V. Vlijmen-Willems, P. Zeeuwen, M.-J. Gerritsen, P. V. D. Kerkhof, P. V. Erp, Epidermal cell kinetics by combining *in situ* hybridization and immunohistochemistry, Histochem. J. 30 (1998) 869–877.

[49] L. Norlén, A. Al-Amoudi, Stratum corneum keratin structure, function, and formation: the cubic rod-packing and membrane templating model, J. Invest. Dermatol. 123 (2004) 715–732.

[50] L. Russell, S. Wiedersberg, M. Delgado-Charro, The determination of stratum corneum thickness: an alternative approach, Eur. J. Pharm. Biopharm. 69 (2008) 861–870.

[51] C. Potten, Epidermal transit times, Br. J. Dermatol. 93 (1975) 649–658.

[52] W. Epstein, H. Maibach, Cell renewal in human epidermis, Arch. Dermatol. 92 (1965) 462–468.

[53] K. Halprin, Epidermal "turnover time" - a re-examination, Br. J. Dermatol. 86 (1972) 14–19.

[54] M. Reiss, L. Lipsey, Z.-L. Zhou, Extracellular calcium-dependent regulation of transmembrane calcium fluxes in murine keratinocytes, J. Cell. Physiol. 147 (1991) 281–291.

[55] J. Meldolesi, T. Pozzan, The endoplasmic reticulum Ca^{2+} store: a view from the lumen, Trends Biochem. Sci. 23 (1998) 10–14.

[56] P. Leinonen, P. Hägg, S. Peltonen, E.-M. Jouhilahti, J. Melkko, T. Korkiamäki, A. Oikarinen, J. Peltonen, Reevaluation of the normal epidermal calcium gradient, and analysis of calcium levels and ATP receptors in Hailey-Hailey and Darier epidermis, J. Invest. Dermatol. 129 (2009) 1379–1387.

[57] J.-K. Cho, D. Bikle, Decrease of Ca^{2+}-ATPase activity in human keratinocytes during calcium-induced differentiation, J. Cell Physiol. 172 (1997) 146–154.

[58] G. Menon, P. Elias, Ultrastructural localization of calcium in psoriatic and normal human epidermis, Arch. Dermatol. 127 (1991) 57–63.

[59] K. Feingold, The role of epidermal lipids in cutaneous permeability barrier homeostasis, J. Lipid Res. 48 (2007) 2531–2546.

[60] M. Kurasawa, T. Maeda, A. Oba, T. Yamamoto, H. Sasaki, Tight junction regulates epidermal calcium ion gradient and differentiation, Biochem. Biophys. Res. Commun. 406 (2011) 506–511.

[61] C. Potten, C. Booth, Keratinocyte stem cells: a commentary, J. Invest. Dermatol. 119 (2002) 888–899.

[62] B. Forslind, G. Roomans, L.-E. Carlsson, K. Malmqvist, K. Akselsson, Elemental analysis on freeze-dried sections of human skin: studies by electron microprobe and particle induced X-ray emission analysis, Scan. Electron Microsc. Pt 2 (1984) 755–759.

[63] N. Grabe, K. Neuber, Simulating psoriasis by altering transit amplifying cells, Bioinformatics 23 (2007) 1309–1312.

[64] G. Topping, J. Malda, R. Dawson, Z. Upton, Development and characterisation of human skin equivalents and their potential application as a burn wound model, Primary Intention 14 (2006) 14–21.

[65] K. Halprin, A. Ohkawara, Glucose entry into the human epidermis: II. The penetration of glucose into the human epidermis *in vitro*, J. Invest. Dermatol. 49 (1967) 561–568.

[66] C. Potten, Epidermal cell production rates, J. Invest. Dermatol. 65 (1975) 488–500.

[67] H. Iizuka, Epidermal turnover time, J. Dermatol. Sci. 8 (1994) 215–217.